Inorganic Chemistry

Article

pubs.acs.org/IC

Syntheses, Structures, and Nonlinear-Optical Properties of Metal Sulfides $Ba_2Ga_8MS_{16}$ (M = Si, Ge)

Bin-Wen Liu,[†] Hui-Yi Zeng,[†] Ming-Jian Zhang,[†] Yu-Hang Fan,[†] Guo-Cong Guo,*[,†] Jin-Shun Huang,[†] and Zhen-Chao Dong*[,‡]

[†]State Key Laboratory of Structural Chemistry, Fujian Institute of Research on the Structure of Matter, Chinese Academy of Sciences, Fuzhou, Fujian 350002, P. R. China

[‡]Hefei National Laboratory for Physical Sciences at the Microscale, University of Science and Technology of China, Hefei, Anhui 230026, P. R. China

Supporting Information

ABSTRACT: Two new metal sulfides, $Ba_2Ga_8MS_{16}$ (M = Si, Ge), have been synthesized by high-temperature solid-state reactions. They are isostructural and crystallize in the noncentrosymmetric space group $P6_3mc$ (No. 186) with a = 10.866(5) Å, c = 11.919(8) Å, and z = 2 for $Ba_2Ga_8SiS_{16}$ (**1**) and a = 10.886(8) Å, c = 11.915(3) Å, and z = 2 for $Ba_2Ga_8GeS_{16}$ (**2**). Their three-dimensional frameworks are constructed by corner-sharing mixed $(Ga/M)S_4$ (M = Si, Ge) and pure GaS_4 tetrahedra, with Ba^{2+} cations filling in the tunnels. Compounds **1** and **2** are transparent over 0.42−20 μm and have wide band gaps of around 3.4 and 3.0 eV, respectively. Polycrystalline **2** displays strong nonlinear second-harmonic-generation (SHG) intensities that are comparable to that of the benchmark $AgGaS_2$ (AGS) with phase-matching behavior at a laser irradiation of 1950 nm. Of particular interest, compound **2** also possesses a high powder laser-induced damage threshold of ~22 times that of AGS. The alternate stacking of the mixed $(Ga/M)S_4$ (M = Si, Ge) tetrahedral layer with the pure GaS_4 tetrahedral layer along the c axis and the alignment of these two types of tetrahedra in the same direction may be responsible for the large SHG signals observed.

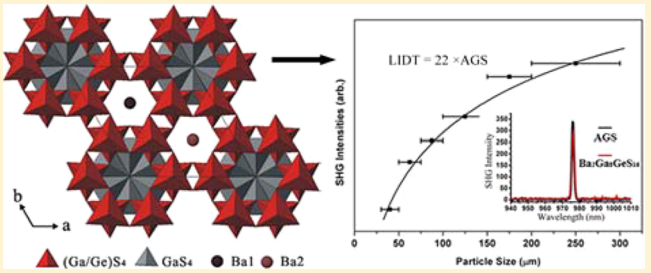

INTRODUCTION

Nonlinear-optical (NLO) materials are important in modern optical science and technology for their applications in laser sources based on the second-harmonic-generation (SHG) and optical parametric oscillation processes.[1] The well-known oxide-based NLO materials such as KH_2PO_4 (KDP), $KTiOPO_4$ (KTP), β-BaB_2O_4 (BBO), and LiB_3O_5 (LBO)[2] are widely used in high-power applications because of their high laser damage thresholds. Nevertheless, their spectral range of good transmission is limited to the UV−vis region, not suitable for the mid- and far-IR region due to strong absorption there. On the other hand, the commercial NLO materials used in the IR region are chalcopyrite semiconductors such as $AgGaS_2$ (AGS), $AgGaSe_2$ (AGSe), and $ZnGeP_2$ (ZGP),[3] which feature high NLO coefficients, but they suffer from relatively low laser-induced damage thresholds (LIDTs) because of their relatively small band gaps, thus limiting their high-power applications in the IR transmission region.[4] Consequently, exploring new NLO materials with both strong nonlinear responses and high LIDTs is still a pressing and important topic in the IR−NLO material field.

The incorporation of an electropositive element such as an alkaline or alkaline-earth element into the framework will widen the band gap of the resulting material, leading to a higher LIDT. Noncentrosymmetric chalcogenides following such a strategy have been investigated as new NLO materials with high LIDTs for IR applications. Related examples include $LiGaS_2$,[5] $LiInS_2$,[6] Li_2CdMS_4 (M = Ge, Sn),[7] $BaGa_4S_7$,[8] $Li_2Ga_2GeS_6$,[9] $Li_2In_2MS_6$ (M = Si, Ge),[10] and $BaGa_2MS_6$ (M = Si, Ge).[11] In this paper, we report a new phase in this largely unexplored AE−III−IV−Q system (AE = alkaline-earth metal; III = Al, Ga, In; IV = Si, Ge, Sn; Q = S, Se), specifically the syntheses, structures, and NLO properties of two metal sulfides, $Ba_2Ga_8SiS_{16}$ (**1**) and $Ba_2Ga_8GeS_{16}$ (**2**).

EXPERIMENTAL SECTION

Syntheses. All starting reactants were handled inside an argon-filled glovebox with controlled oxygen and moisture levels below 0.1 ppm. Ba metal (99.9%), Ga_2O_3 powder (99.9%), Ge powder (99.99%), Si powder (99.99%), S powder (99.99%), and B powder (99.99%) were used as received without further purification. The binary starting material, Ga_2S_3, was synthesized as a precursor, which was obtained from a stoichiometric mixture of the elements B and S and compound Ga_2O_3, then annealed at 950 °C for 2 days, and finally cooled to room temperature (the use of B is to take away the O component in the starting material). For the synthesis of target

Special Issue: To Honor the Memory of Prof. John D. Corbett

Received: September 28, 2014

   dx.doi.org/10.1021/ic502362f | Inorg. Chem. XXXX, XXX, XXX−XXX

compounds, a stoichiometric mixture with an overall weight of about 300 mg of the starting materials Ba, Ga_2S_3, Ge (Si), and S in a molar ratio of 2:4:1:4 was loaded into a quartz tube and then flame-sealed under vacuum (~10^{-4} Torr). The tube was then placed in a temperature-controlled muffle furnace, held at 300 °C for 5 h, then heated to 650 °C for over 5 h and kept there for 10 h, subsequently heated to 980 °C for over 10 h, dwelled for 5 days, and finally slowly cooled to 400 °C before the furnace power was switched off. Transparent yellow single crystals of the title compounds were obtained in high purity and were stable in air for several months.

Single-Crystal X-ray Diffraction (XRD). Single-crystal XRD data were performed on a Rigaku Mercury CCD diffractometer equipped with graphite-monochromated Mo Kα radiation (λ = 0.71073 Å) at 293 K. The intensity data sets were collected using a ω-scan technique and reduced using *CrystalClear* software.[12] The structures were solved by direct methods and refined by full-matrix least-squares methods on F^2 with anisotropic thermal parameters for all atoms. All of the calculations were performed with the Siemens *SHELXTL*, version 5, package of crystallographic software.[13] The space group was determined to be $P6_3mc$, based on the intensity distribution and systematic extinction of the observed structure factors. The final structures were examined for additional symmetry with *ADDSYM/PLATON*.[14] The assignment of the Ba and S atoms in both structures can be readily done assuming that these atoms take over the corresponding crystallographic positions with full occupancy. However, the assignment of crystallographic sites M1 (12d) and M2 (6c) to Ga or Si (Ge) or a mixture of them needs careful consideration. Taking compound **2** as an example, on the basis of a molar ratio of Ga:Ge close to 8:1 in terms of energy-dispersive X-ray (EDX) measurement results and the charge-balance requirement for a neutral compound, the M1 site was assigned to a mixed occupancy of Ga/Ge with a partial occupancy of 0.833(3)/0.166(7) and the M2 site to pure Ga, thus generating a consistent chemical formula of $Ba_2Ga_8GeS_{16}$. The above assignments can be further supported by calculating the valence bond sums (VBSs)[15] around each site, which suggests that that the M1 site is partially filled by Ga and Ge (VBS = 3.17) and the M2 site is fully occupied by Ga (VBS = 3.01). Similar procedures were applied for the structural determination of **1**. Because Si is much lighter (or smaller) than Ga, a judgment in terms of reasonable amplitude of the isotropic thermal parameters for different assignments of atoms to the M1 or M2 sites also favors the mixed-occupancy model proposed above for compound **2**. The program *STRUCTURE TIDY*[16] was used to put the positional parameters in a standard setting. Additional crystallographic details are given in Table 1, the selected bond distances and bond angles are given in Table 2, and the positional coordinates and isotropic equivalent thermal parameters are listed in Table S1 in the Supporting Information (SI). Further information may be found in the SI.

Table 1. Crystal Data and Structure Refinements for 1 and 2

empirical formula	$Ba_2Ga_8SiS_{16}$ (**1**)	$Ba_2Ga_8GeS_{16}$ (**2**)
fw	1373.49	1417.99
temperature (K)	293(2)	293(2)
space group	$P6_3mc$	$P6_3mc$
a (Å)	10.866(5)	10.886(8)
c (Å)	11.919(8)	11.915(3)
γ (deg)	120	120
V (Å^3)	1218.8(1)	1223.0(1)
Z	2	2
D_{calcd} (g cm^{-3})	3.743	3.851
μ (mm^{-1})	13.279	14.389
GOF on F^2	1.062	1.039
$R_1{}^a$ [$I > 2\sigma(I)$]	0.0230	0.0150
$wR_2{}^b$ [$I > 2\sigma(I)$]	0.0463	0.0272
$R_1{}^a$ (all data)	0.0248	0.0164
$wR_2{}^b$ (all data)	0.0469	0.0280
Flack parameter x	0.004(2)	0.000(1)
$\Delta\rho_{max}/\Delta\rho_{min}$ (e Å^{-3})	0.766/−0.797	0.457/−0.431

$^aR_1 = \sum||F_o| - |F_c||/\sum|F_o|$. $^bwR_2 = \sum[(w(F_o^2 - F_c^2)^2]/\sum[w(F_o^2)^2)]^{1/2}$.

Table 2. Selected Interatomic Distances (Å) and Bond Angles (deg) in 1 (M = Si) and 2 (M = Ge)

	1	2
	Bond Lengths	
Ba1−S2 (×3)	3.454(2)	3.442(1)
Ba1−S3 (×3)	3.567(3)	3.554(1)
Ba1−S1 (×6)	3.597(2)	3.606(7)
Ba2−S1 (×6)	3.531(2)	3.533(8)
Ba2−S3 (×6)	3.606(3)	3.603(1)
Ba2−S2 (×3)	3.659(3)	3.655(1)
Ga/M1−S2	2.230(2)	2.248(8)
Ga/M1−S3	2.237(2)	2.252(8)
Ga/M1−S1	2.253(2)	2.254(1)
Ga/M1−S4	2.312(1)	2.322(7)
Ga2−S1 (×2)	2.241(2)	2.244(8)
Ga2−S5	2.303(2)	2.307(9)
Ga2−S4	2.324(2)	2.320(1)
	Bond Angles	
S2−Ga/M1−S3	114.13(7)	113.90(4)
S2−Ga/M1−S1	110.63(7)	110.62(4)
S3−Ga/M1−S1	104.59(7)	104.48(4)
S2−Ga/M1−S4	109.85(7)	109.86(4)
S3−Ga/M1−S4	107.68(6)	107.70(4)
S1−Ga/M1−S4	109.78(7)	110.12(4)
S1−Ga2−S1	110.35(7)	110.30(5)
S1−Ga2−S5	111.07(7)	111.25(4)
S1−Ga2−S5	111.07(7)	111.25(4)
S1−Ga2−S4	108.44(5)	108.41(4)
S1−Ga2−S4	108.44(5)	108.41(4)
S5−Ga2−S4	107.34(9)	107.09(6)

Powder XRD. To make phase characterization and identification, powder XRD data of samples **1** and **2** were recorded on an automated Rigaku MiniFlex II X-ray diffractometer equipped with a diffracted monochromator set for Cu Kα radiation (λ = 1.54057 Å), operating at 30 kV and 40 mA. The observed powder patterns were found to be in good agreement with the simulated ones based on the single-crystal structure refinements of **1** and **2**, respectively (Figure S1 in the SI). Such an agreement suggests that the crystals are quite pure, particularly for phase **2**, despite the possible existence of a tiny amount of GaS ($P6_3/mmc$) in phase **1**. Compound **2** also turns out to be a high-yield phase (>80%). Therefore, the measurements of the optical properties were mainly carried out for **2**.

EDX Measurements. Semiquantitative EDX was performed with an EDX-equipped Hitachi S-3500 scanning electron microscopy spectrometer on the crystal that was used for single-crystal XRD. The measurements confirmed the presence of Ba, Ga, Si (Ge), and S in an approximate molar ratio of 2:8:1:16 (Figures S2 and S3 in the SI). No other elements were detected.

IR and UV−Vis−Near-IR (NIR) Diffuse-Reflectance Spectroscopy. The optical diffuse-reflectance spectra of powder samples **1** and **2** were measured at room temperature using a PerkinElmer Lambda 900 UV−vis spectrophotometer equipped with an integrating sphere attachment and $BaSO_4$ as the reference. The absorption spectra were calculated from the reflection spectra using the Kubelka−Munk formula: $\alpha/S = (1-R)^2/2R$,[17] in which α is the absorption coefficient, S is the scattering coefficient, and R is the reflectance. IR spectra were recorded using a Nicolet Magana 750 Fourier transform IR spectrophotometer in the range 4000−500 cm^{-1}. Powdery samples were diluted with dry KBr and pressed into pellets before measurements.

dx.doi.org/10.1021/ic502362f | Inorg. Chem. XXXX, XXX, XXX−XXX

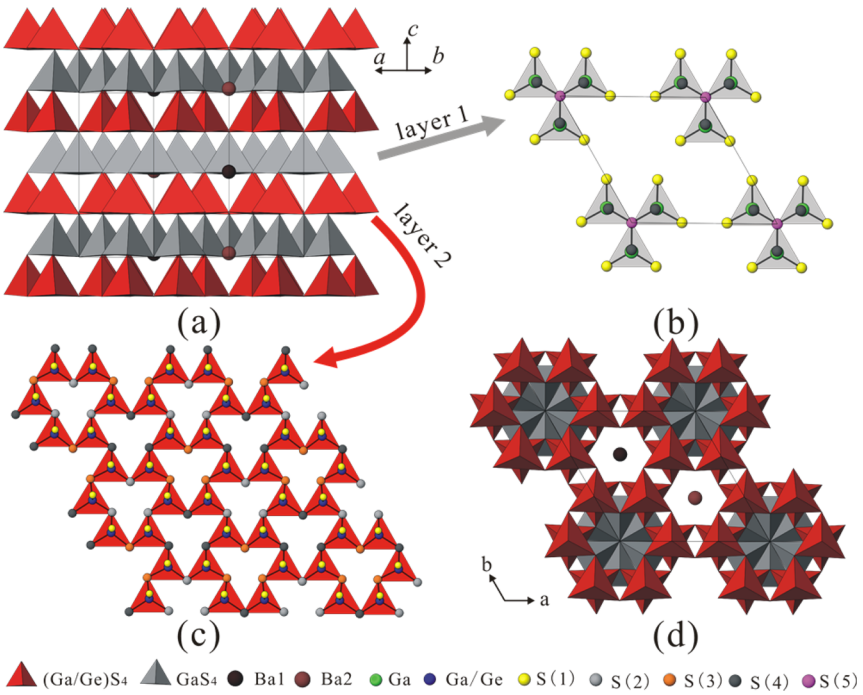

Figure 1. Crystal structure of **2**. (a) 3D framework showing alternate stacking of two types of tetrahedral layers. (b) Tetrahedral layer constructed by the pure GaS_4 tetrahedra. (c) Tetrahedral layer made up of mixed $(Ga/Ge)S_4$ tetrahedra. (d) 3D framework viewed along the *c* axis.

SHG Measurements. The powder SHG measurement of **2** was investigated using a modified Kurtz–Perry powder technique under laser irradiation at 1950 nm. Microcrystalline samples were sieved into several distinct particle size ranges (30–50, 50–75, 75–100, 100–150, 150–200, and 200–300 μm) for the SHG phase-matching measurements. The crystalline sample of AGS with similar particle sizes served as the standard. The frequency-doubling signals (975 nm) were detected by an Andor DU420A-BR-DD CCD.

LIDT Measurements.[18] The powder LIDT measurement of **2** was performed on a microcrystalline sample (200–300 μm), with a focused high-power 1064 nm laser beam with a pulse width τ_p of 8 ns and a repetition rate of 1 Hz. Microcrystalline AGS of a similar particle size (200–300 μm) was used as the reference. The power of the laser beam was measured by a Nova II sensor display with a PE50-DIF-C energy sensor. An optical concave lens was used to adjust the diameter of the laser beam to obtain different intensities. The measurements were carried out by gradually increasing the laser power until the color of the sample changed, at which time the laser power was defined as the damage threshold. The area of the damage spot was then measured to estimate the value of the LIDT.

Electronic Band Structure Calculation. Preliminary calculations of electronic band structures are also performed for **1** and **2** based on the structures determined by single-crystal XRD analysis. The CASTEP code on the basis of density functional theory was used to calculate band structures and densities of state (DOSs) using a plane-wave expansion of the wave functions and an ultrasoft pseudopotential,[19] in which the orbital electrons of Ba $4d^{10}5s^25p^66s^2$, Ga $3d^{10}4s^24p^1$, Ge $4s^24p^2$, Si $3s^23p^2$, and S $3s^23p^4$ were treated as valence electrons. The number of plane waves included on this basis was determined using a cutoff energy of 295 eV, and the numerical integration of the Brillouin zone was performed using a 1 × 1 × 1 Monkhorst–Pack *k*-point sampling.

RESULTS AND DISCUSSION

Crystal Structures. The metal sulfides **1** and **2** are isostructural and crystallize in the noncentrosymmetric space group $P6_3mc$ (No. 186). In the asymmetric unit, there are two crystallographically independent Ba atoms, five S atoms, one Ga atom, and one position partially filled by Ga and M (M = Si, Ge) with an occupancy ratio of Ga:M = 5:1.

Both compounds adopt the same three-dimensional (3D) framework structure that consists of alternate stacking of two distinct tetrahedral layers (Figure 1a). Taking compound **2** as an example, one layer is constructed by pure GaS_4 tetrahedral units, in which each Ga atom is coordinated by two S1, one S4, and one S5 atoms in a slightly distorted tetrahedral coordination geometry and every three neighboring GaS_4 tetrahedra are condensed into a trimeric $Ga_3S1_6S4_3S5$ unit (Figure 1b). The other tetrahedral layer is built up from mixed $(Ga/Ge)S_4$ tetrahedral units, in which each Ga/Ge atom is coordinated by one S1, one S2, one S3, and one S4 atoms in a disordered tetrahedral environment. The $(Ga/Ge)S_4$ tetrahedra are interconnected by corner-sharing S2, S3, and S4 atoms in the *ab* plane, forming a $^2_\infty[(Ga/Ge)_6S1_6S2_{6/2}S3_{6/2}S4_{6/2}]$ layer (Figure 1c). The pure GaS_4 and mixed $(Ga/Ge)S_4$ layers are stacked alternately along the [0 0 1] direction via sharing S1 and S4 atoms, with neighboring GaS_4 and $(Ga/Ge)S_4$ layers revolving 60° against each other (Figure 1d). The above condensation of tetrahedral units results in a 3D anion framework of $^3_\infty[Ga_8GeS_{16}]^{-4}$, which is charge-balanced by two Ba^{2+} cations residing in the tunnels along the *c* direction and at one of the interfaces between the pure GaS_4 and mixed $(Ga/Ge)S_4$ layers (Figure 1a,d). Each Ba ion is coordinated to 12 S atoms to form a tetrakadecahedron with Ba–S distances ranging over 3.44–3.66 Å, comparable to those observed in $BaGa_4S_7$[8] and $BaGa_2GeS_6$.[11] Nevertheless, both Ba^{2+} cations are slightly off the interstitial center positions, as evidenced by the asymmetry in the bond lengths (Figure 2).

Overall speaking, as listed in Table 2, the metal–sulfur distances in both the pure GaS_4 and mixed $(Ga/Ge)S_4$ tetradedra vary over a similar range of 2.24–2.32 Å. Nevertheless, in comparison with the pure GaS_4 tetrahedron, the mixed $(Ga/Ge)S_4$ tetrahedron appears slightly more distorted, judging from the slightly larger variations in the

dx.doi.org/10.1021/ic502362f | Inorg. Chem. XXXX, XXX, XXX–XXX

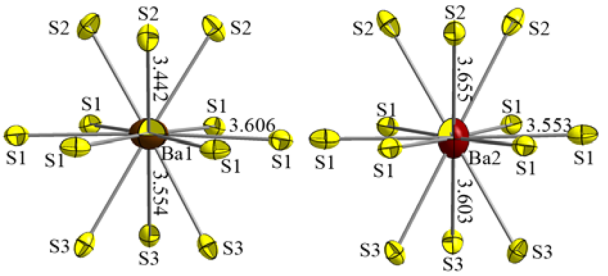

Figure 2. View of the anisotropic thermal ellipsoids (95% probability level) of Ba atoms in **2** with Ba–S distances marked.

bond angles, 107–111° for the pure S–Ga–S and 105–114° for the mixed S–Ga/Ge–S. In addition, the Ga/Ge–S bond distances in **2** are slightly larger than the corresponding Ga/Si–S bond distances in **1**, in agreement with the larger size of Ge than Si. Both bond distances and bond angles observed here are consistent with those reported in $Ba_4CuGa_5S_{12}$,[20] Li_2CdGeS_4,[7] and $Eu_2Ga_2GeS_8$,[21] but the structural variations on the tetrahedral distortion and bond lengths give further justification to the successful assignment of Si or Ge to the crystallographic M1 (12d) sites. Such an assignment leads to a crystal structure that features alternate stacking of the mixed $(Ga/Ge)S_4$ and pure GaS_4 tetrahedral layers along the *c* axis, which, in combination with the alignment of these two types of tetrahedra in the same direction and probably also the slight off-center feature of alkaline-earth cations inside the interstitials, may modify the electronic (or charge) distribution of the structure. An enhanced capability of light polarization may thus be obtained and may be responsible for the large nonlinear SHG signals observed experimentally (see below for detailed results).

IR and UV–Vis–NIR Diffuse-Reflectance Spectroscopy. The UV–vis–NIR diffuse-reflectance spectra in Figure 3 show strong absorption edges roughly at 3.4 and 3.0 eV respectively for **1** (Figure 3a) and **2** (Figure 3b). In comparison to the values of AGS (2.64 eV) and ZGP (1.75 eV), compounds **1** and **2** have relatively wide band gaps, indicating that they may have high LIDTs. The present compounds exhibit high transparency in a broad spectral range from 0.42 to 20 μm (Figures 3 and S4 in the SI), which covers the important band ranges of 3–5 and 8–14 μm of atmospheric transparent windows. All of these observations suggest that they may be suitable for a variety of NLO applications in longer-wavelength (mid/far-IR) regions.

SHG. The SHG signals as a function of the particle size from the measurements made on ground crystals for **2** are shown in Figure 4; the SHG intensities increase with increasing particle size and then reach a plateau at the maximum value after a certain particle size. Such a correlation is consistent with a phase-matching behavior for the nonlinear frequency-doubling signals at 975 nm induced by the incident laser at 1950 nm (Figure 4), according to the rule proposed by Kurtz and Perry.[22] A sample of AGS (200–300 μm) was also prepared as a reference material. The measured SHG intensities of **2** are 0.9 times that of AGS (d_{eff} = ~13.7 pm V^{-1};[23] see the inset in Figure 4). It is known that the measured SHG signal intensity by the Kurtz and Perry powder method is proportional to the square of the SHG coefficient d_{eff}, and the second-order susceptibility $\chi^{(2)}_{eff}$ is twice that of the SHG coefficient d_{eff}. Therefore, the estimated second-order susceptibility $\chi^{(2)}_{eff}$ for **2** is ~26 pm V^{-1}.

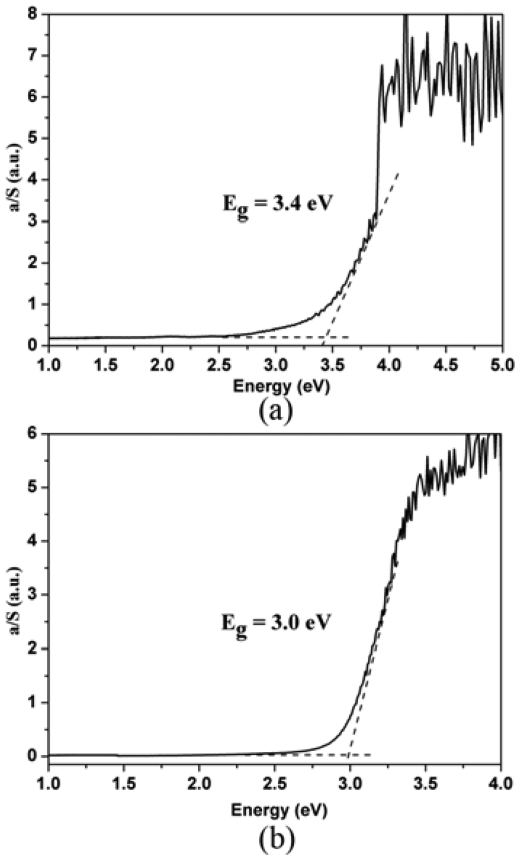

Figure 3. UV–vis diffuse-reflectance spectra of **1** (a) and **2** (b).

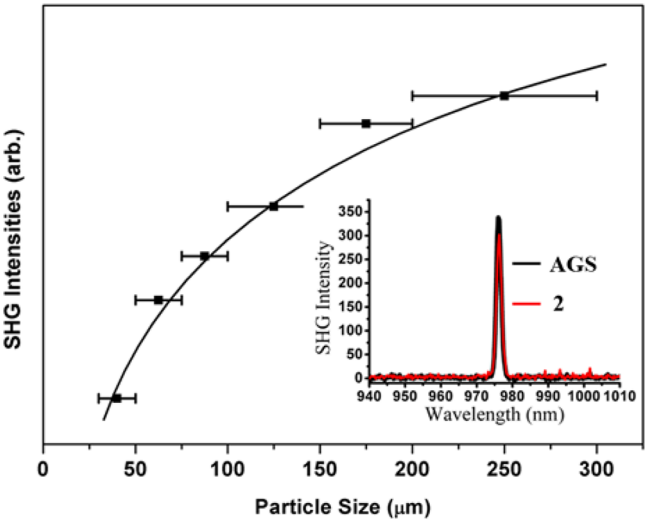

Figure 4. Phase-matching results for **2**. The curve is to guide the eye and is not a fit to the data. Inset: SHG signals of **2** and AGS.

Powder LIDT. The powder LIDT data of **2** and AGS measured by the single-pulse powder LIDT method are shown in Table 3. The threshold of the laser power for the onset

Table 3. Powder LIDTs

compound	damage energy (mJ)	spot diameter (mm)	τ_p (ns)	damage threshold [MW cm^{-2}]
2	19.0	1.9	8	83.8
AGS	4.8	4.5	8	3.8

dx.doi.org/10.1021/ic502362f | *Inorg. Chem.* XXXX, XXX, XXX–XXX

damage of sample **2** (19.0 mJ) is much larger than that of AGS (4.8 mJ). So, a smaller spot diameter (1.9 mm) was selected for **2**, in comparison with the 4.5 mm value for the AGS sample. The damage thresholds of **2** and AGS were derived from the equation $I_{threshold} = E/\pi r^2\tau_p$, in which E is the laser energy of a single pulse, r is the spot radius, and τ_p is the pulse width. The sample color of compound **2** was changed from yellow to black upon laser illumination for about 1 s. The LIDT thus estimated for phase **2** was roughly 84 MW cm^{-2}, ~22 times of that of AGS (3.8 MW cm^{-2}), which indicates that compound **2** may be a good candidate for high-power IR–NLO applications. The laser damage mechanism is still unclear, but given the observed band gap of 3.0 eV for compound **2**, this phase should be able to sustain laser illumination at 1064 nm without invoking two-photon absorption problems.

Electronic Band Structure Calculations. Figure 5 plots the calculated electronic band structures of **1** and **2** along high

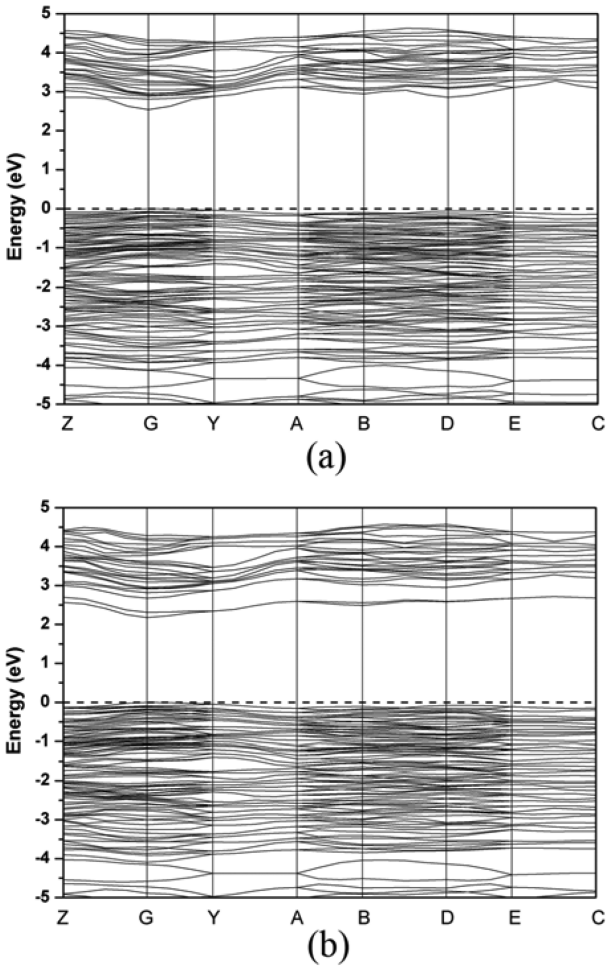

Figure 5. Band structures of **1** (a) and **2** (b). The Fermi level is set at 0 eV for all of the band structures and DOS.

symmetry points of the first Brillouin zone. According to the calculated band diagrams, they are direct-band-gap materials with band gaps at ~2.5 and ~2.2 eV respectively for **1** and **2**. Note that these band gaps are smaller than the corresponding experimental values of ~3.4 and ~3.0 eV derived from the UV–vis diffuse-reflectance spectra presumably due to the inaccurate description of the eigenvalues of the electronic states in the generalized gradient approximation. A slightly smaller band gap for phase **2** may be related to stronger state hybridization between the Ge and S atoms in comparison with the Si–S interaction for phase **1**.

The band components of **1** and **2** are shown by the total and partial DOSs in Figure 6. The conduction band is mostly

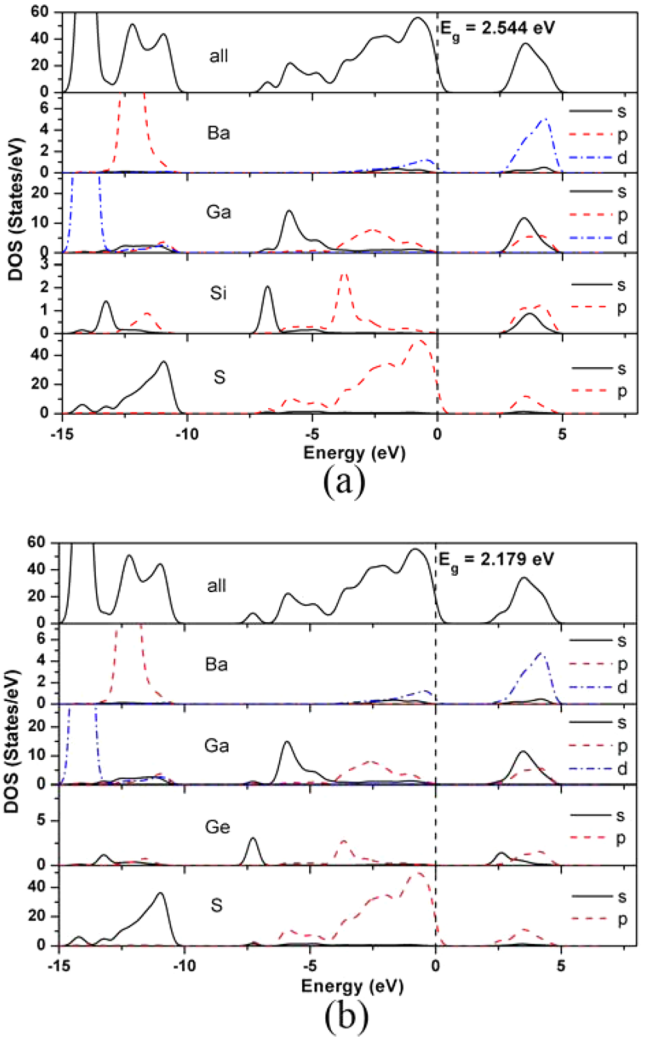

Figure 6. Total and partial DOSs of **1** (a) and **2** (b). The Fermi level is set at 0 eV for all of the band structures and DOS.

composed of Ga 4s and S 3p states, mixing with small amounts of Ba 5d, Ga 4p, Ge 4s (Si 3s), and Ge 4p (Si 3p) states, while the valence band from −8.0 eV to the Fermi level originates predominately from S 3p and Ga 4s states, mixing with small amounts of Ga 4p, Ge 4s (Si 3s), and Ge 4p (Si 3p) states. The band from −15.0 to −8.0 eV was mainly composed of Ga 3d and S 3s states, as well as a small portion of Ba 6s and Ge 4s (Si 3s) states. Therefore, their optical absorptions can mainly be ascribed to the charge transfer (or charge density oscillation) from S 3p states to Ga 4s and Ga 4p states. Nevertheless, we should note that the current calculation is still preliminary, providing only a qualitative picture about their band structure and DOS distribution. More sophisticated modeling and calculations are still needed in order to figure out the correlation between the crystal structure, electronic band structure, and NLO properties observed.

dx.doi.org/10.1021/ic502362f | Inorg. Chem. XXXX, XXX, XXX–XXX

CONCLUSION

In summary, two new metal sufides, $Ba_2Ga_8MS_{16}$ (**1**, M = Si; **2**, M = Ge), were obtained via high-temperature solid-state reactions. They are isostructural and crystallize in the noncentrosymetric hexagonal space group $P6_3mc$. Their 3D frameworks are constructed by alternate layer stacking via corner sharing in both the pure GaS_4 and mixed $(Ga/M)S_4$ (M = Si, Ge) tetrahedral layers. Compounds **1** and **2** both have wide-IR transparent regions and large band gaps. Furthermore, phase **2** exhibits strong SHG signals that are comparable to those of the benchmark AGS at laser irradiation of 1950 nm. The powder LIDT measurements indicate a high LIDT for **2**, ~22 times that of AGS. The observed large nonlinear signals are presumably related to the synergic action of the alternate stacking of the mixed $(Ga/Ge)S_4$ and the pure GaS_4 tetrahedral layers along the *c* axis, the alignment of these two types of tetrahedra in the same direction, and the slight off-center feature of alkaline-earth cations in the interstitial sites. These structural factors may modify the charge distribution of the structure and result in an enhanced performance in light polarization. Our results indicate that **2** can be a good candidate for high-power IR–NLO applications.

ASSOCIATED CONTENT

Supporting Information

CIF data and additional tables and figures. This material is available free of charge via the Internet at http://pubs.acs.org.

AUTHOR INFORMATION

Corresponding Authors

*E-mail: gcguo@fjirsm.ac.cn.
*E-mail: zcdong@ustc.edu.cn.

Notes

The authors declare no competing financial interest.

ACKNOWLEDGMENTS

We gratefully acknowledge financial support by the NSF of China (Grants 91222204, 21403231, 21101152, and 91021004), the Key Project from the CAS (Grant KJCX2-EW-H03), and the NSF of Fujian Province (Grant 2014J05025).

REFERENCES

(1) (a) Serebryakov, V. A.; Boiko, E. V.; Petrishchev, N. N.; Yan, A. V. *J. Opt. Technol.* **2010**, *77*, 6–17. (b) Chen, W.; Mouret, G.; Boucher, D.; Tittel, F. K. *Appl. Phys. B: Laser Opt.* **2001**, *72*, 873–876. (c) Chen, C. T.; Liu, G. Z. *Annu. Rev. Mater. Sci.* **1986**, *16*, 203–243. (d) Pauzauskie, P. J.; Yang, P. *Mater. Today* **2006**, *9*, 36–45. (e) Bordui, P. F.; Fejer, M. M. *Annu. Rev. Mater. Sci.* **1993**, *23*, 321–379.

(2) (a) Chen, C. T.; Wu, B. C.; Jiang, A. D.; You, G. M. *Sci. Sin., Ser. B* **1985**, *28*, 235–243. (b) Tang, C. L.; Bosenberg, W. R.; Ukachi, T.; Lane, R. J.; Cheng, L. K. *Proc. IEEE* **1992**, *80*, 365–374. (c) Smith, W. L. *Appl. Opt.* **1977**, *16*, 798. (d) Kato, K. *IEEE J. Quantum Electron.* **1991**, *27*, 1137–1140.

(3) (a) Chemla, D. S.; Kupecek, P. J.; Robertson, D. S.; Smith, R. C. *Opt. Commun.* **1971**, *3*, 29–31. (b) Boyd, G. D.; Kasper, H. M.; McFee, J. H.; Storz, F. G. *IEEE J. Quantum Electron.* **1972**, *QE-8*, 900–908. (c) Boyd, G. D.; Buehler, E.; Storz, F. G. *Appl. Phys. Lett.* **1971**, *18*, 301–304. (d) Okorogu, A. O.; Mirov, S. B.; Lee, W.; Crouthamel, D. I.; Jenkins, N.; Dergachev, A. Y.; Vodopyanov, K. L.; Badikov, V. V. *Opt. Commun.* **1998**, *155*, 307–312. (e) Chung, I.; Kanatzidis, M. G. *Chem. Mater.* **2014**, *26*, 849–869.

(4) Giles, N. C.; Bai, L. H.; Chirila, M. M.; Garces, N. Y.; Stevens, K. T.; Schunemann, P. G.; Setzler, S. D.; Pollak, T. M. *J. Appl. Phys.* **2003**, *93*, 8975–8981.

(5) Isaenko, L.; Yelisseyev, A.; Lobanov, S.; Krinitsin, P.; Petrov, V.; Zondy, J. J. *J. Non-Cryst. Solids* **2006**, *352*, 2439–2443.

(6) Isaenko, L.; Vasilyeva, I.; Merkulov, A.; Yelisseyev, A.; Lobanov, S. *J. Cryst. Growth* **2005**, *275*, 217–223.

(7) (a) Lekse, J. W.; Moreau, M. A.; McNerny, K. L.; Yeon, J.; Halasyamani, P. S.; Aitken, J. A. *Inorg. Chem.* **2009**, *48*, 7516–7518. (b) Brant, J. A.; Clark, D. J.; Kim, Y. S.; Jang, J. Y.; Zhang, J. H.; Aitken, J. A. *Chem. Mater.* **2014**, *26*, 3045–3048.

(8) Lin, X. S.; Zhang, G.; Ye, N. *Cryst. Growth Des.* **2009**, *9*, 1186–1189.

(9) Kim, Y.; Seo, I. S.; Martin, S. W.; Baek, J.; Halasyamani, P. S.; Arumugam, N.; Steinfink, H. *Chem. Mater.* **2008**, *20*, 6048–6052.

(10) Yin, W. L.; Feng, K.; Hao, W. Y.; Yao, J. Y.; Wu, Y. C. *Inorg. Chem.* **2012**, *51*, 5839–5843.

(11) (a) Lin, X. S.; Guo, Y. F.; Ye, N. *J. Solid State Chem.* **2012**, *195*, 172–177. (b) Yin, W. L.; Feng, K.; He, R.; Mei, D. J.; Lin, Z. S.; Yao, J. Y.; Wu, Y. C. *Dalton Trans.* **2012**, *41*, 5653–5661.

(12) *CrystalClear*, version 1.3.5; Rigaku Corp.: Tokyo, 2002.

(13) *SHELXTL Reference Manual*, version 5; Siemens Energy & Automation Inc.: Madison, WI, 1994.

(14) Spek, A. L. *PLATON, A Multipurpose Crystallographic Tool*; Utrecht University: Utrecht, The Netherlands, 2005.

(15) (a) Brese, N. E.; Keeffe, M. O. *Acta Crystallogr., Sect. B: Struct. Sci.* **1991**, *47*, 192–197. (b) Chen, Y. K.; Chen, M. C.; Zhou, L. J.; Chen, L.; Wu, L. M. *Inorg. Chem.* **2013**, *52*, 8334–8341. (c) Mei, D. J.; Yin, W. L.; Feng, K.; Lin, Z. S.; Bai, L.; Yao, J. Y.; Wu, Y. C. *Inorg. Chem.* **2012**, *51*, 1035–1040.

(16) Gelato, L. M.; Parthé, E. *J. Appl. Crystallogr.* **1987**, *20*, 139–143.

(17) Korum, G. *Reflectance Spectroscopy*; Springer: New York, 1969.

(18) (a) Zhang, G.; Li, Y. J.; Jiang, K.; Zeng, H. Y.; Liu, T.; Chen, X. G.; Qin, J. G.; Lin, Z. S.; Fu, P. Z.; Wu, Y. C.; Chen, C. T. *J. Am. Chem. Soc.* **2012**, *134*, 14818–14822. (b) Zhang, M.-J.; Jiang, X.-M.; Zhou, L.-J.; Guo, G.-C. *J. Mater. Chem. C* **2013**, *1*, 4754–4760. (c) Zhang, M.-J.; Li, B.-X.; Liu, B.-W.; Fan, Y.-H.; Li, X.-G.; Zeng, H.-Y.; Guo, G.-C. *Dalton Trans.* **2013**, *42*, 14223–14229.

(19) (a) Hamann, D. R.; Schluter, M.; Chiang, C. *Phys. Rev. Lett.* **1979**, *43*, 1494–1497. (b) Segall, M. M.; Linda, P. J. D; Probert, M. J.; Pickard, C. J.; Hasnip, P. J.; Clark, S. J.; Payne, M. C. *J. Phys.: Condens. Matter* **2002**, *14*, 2717–2744. (c) Perdew, J. P.; Burke, K.; Ernzerhof, M. *Phys. Rev. Lett.* **1996**, *77*, 3865–3868.

(20) Kuo, S. M.; Chang, Y. M.; Chung, M.; Jang, J. I.; Her, B. H.; Yang, S. H.; Ketterson, J. B.; Kanatzidis, M. G.; Hsu, K. F. *Chem. Mater.* **2013**, *25*, 2427–2433.

(21) Chen, M. C.; Li, P.; Zhou, L. J.; Li, L. H.; Chen, L. *Inorg. Chem.* **2011**, *50*, 12402–12404.

(22) Kurtz, S. K.; Perry, T. T. *J. Appl. Phys.* **1968**, *39*, 3798–3813.

(23) Zondy, J. J.; Touahri, D.; Acef, O. *J. Opt. Soc. Am. B* **1997**, *14*, 2481–2497.